Tracking S4 movement by gating pore currents in the bacterial sodium channel NaChBac

Tamer M. Gamal El-Din, Todd Scheuer, and William A. Catterall

Department of Pharmacology, University of Washington, Seattle, WA 98195

Voltage-gated sodium channels mediate the initiation and propagation of action potentials in excitable cells. Transmembrane segment S4 of voltage-gated sodium channels resides in a gating pore where it senses the membrane potential and controls channel gating. Substitution of individual S4 arginine gating charges (R1–R3) with smaller amino acids allows ionic currents to flow through the mutant gating pore, and these gating pore currents are pathogenic in some skeletal muscle periodic paralysis syndromes. The voltage dependence of gating pore currents provides information about the transmembrane position of the gating charges as S4 moves in response to membrane potential. Here we studied gating pore current in mutants of the homotetrameric bacterial sodium channel NaChBac in which individual arginine gating charges were replaced by cysteine. Gating pore current was observed for each mutant channel, but with different voltage-dependent properties. Mutating the first (R1C) or second (R2C) arginine to cysteine resulted in gating pore current at hyperpolarized membrane potentials, where the channels are in resting states, but not at depolarized potentials, where the channels are activated. Conversely, the R3C gating pore is closed at hyperpolarized membrane potentials and opens with channel activation. Negative conditioning pulses revealed time-dependent deactivation of the R3C gating pore at the most hyperpolarized potentials. Our results show sequential voltage dependence of activation of gating pore current from R1 to R3 and support stepwise outward movement of the substituted cysteines through the narrow portion of the gating pore that is sealed by the arginine side chains in the wild-type channel. This pattern of voltage dependence of gating pore current is consistent with a sliding movement of the S4 helix through the gating pore. Through comparison with high-resolution models of the voltage sensor of bacterial sodium channels, these results shed light on the structural basis for pathogenic gating pore currents in periodic paralysis syndromes.

The Journal of General Physiology

INTRODUCTION

Voltage-gated sodium channels are complex transmembrane proteins that sense the membrane electric field and open a central pore that conducts ions across the membrane and initiates action potentials in excitable cells (Hille, 2001). They are composed of four subunits or domains that each contain six transmembrane segments (S1–S6). The S1–S4 segments comprise the voltage-sensing module, whereas the S5 and S6 segments and the intervening P loop comprise the pore module (Catterall, 2000). Transmembrane segment S4 has positively charged amino acid residues at every third position, which serve as the gating charges of the channels (Stühmer et al., 1989). Electrostatic force exerted on these gating charges by the membrane potential induces conformational changes in the channel protein and drives it from resting to activated and inactivated states (Bezanilla, 2000; Catterall, 2000, 2010). The efficiency of electromechanical coupling depends on transduction of the electrical force on the S4 segment, which induces its outward movement, into a mechanical force applied to the S4–S5 linker to open the pore. The S4 segment and its gating charges move outward across the membrane in response to depolarization (Yang and Horn, 1995; Yang et al., 1996). For efficient translocation of gating charges, the movement of the S4 segment must follow a low energy path across the membrane, which is provided by its sliding movement through a gating pore formed by the S1–S3 segments (Catterall, 2000, 2010). The gating pore focuses the transmembrane electric field to a distance of ∼5 Å normal to the membrane (Yang et al., 1996; Starace and Bezanilla, 2004). Up to 14 electrical charges move across the electric field to open eukaryotic sodium channels (Conti and Stühmer, 1989; Hirschberg et al., 1995; Gamal El-Din et al., 2008), and ∼16 charges act to open the bacterial sodium channel NaChBac (Kuzmenkin et al., 2004).

The crystal structures of voltage-gated sodium and potassium channels revealed that the S1–S3 segments surround S4 and create a gating pore in the voltage sensor through which the gating charges can move easily (Long et al., 2005, 2007; Payandeh et al., 2011). The arginine gating charges form salt bridges and hydrogen bonds with neighboring negative charges and hydrophilic residues in the S1–S3 transmembrane segments

Correspondence to William A. Catterall: wcatt@uw.edu

The Rockefeller University Press $30.00
J. Gen. Physiol. Vol. 144 No. 2 147–157
www.jgp.org/cgi/doi/10.1085/jgp.201411210

(Catterall, 2000, 2010; Long et al., 2007; Payandeh et al., 2011). The structures of the voltage sensors revealed a transmembrane position for the S4 segment, with its outer gating charges interacting with negatively charged or hydrophilic residues in the extracellular negative cluster, its gating charge R3 placed in or near the hydrophobic constriction site which seals the voltage sensor from transmembrane movement of water and ions, and its gating charge R4 interacting with an intracellular negative cluster of amino acid residues (Long et al., 2005, 2007; Payandeh et al., 2011). Mutations of sodium channel gating charges R1, R2, and R3 to smaller, hydrophilic residues allows state-dependent leak conductance of ions through the mutant voltage sensors (Sokolov et al., 2005, 2007, 2008). Single-residue substitutions generate a low-conductance leak, whereas double substitutions of two adjacent gating charges induce much larger gating pore currents (Sokolov et al., 2005; Gamal El-Din et al., 2010). The small gating-pore leak current caused by single substitutions for gating charges R1, R2, and R3 causes hypokalemic periodic paralysis and normokalemic periodic paralysis (Sokolov et al., 2007, 2008, 2010; Struyk and Cannon, 2007).

The bacterial sodium channel NaChBac is a homotetrameric channel from *Bacillus halodurans* (Ren et al., 2001). It provides an ideal model for structure–function studies of sodium channels because of its small size and homotetrameric organization. We have taken advantage of this simple structure to elucidate the sequence of outward movement of the R1, R2, and R3 gating charges by measurement of gating pore currents. State-dependent activation and deactivation of gating pore currents allowed us to assess the entry into and exit from the gating pore by each gating charge. Our results show that R1 and R2 occupy the gating pore in the resting state. R3 replaces them in the activated state. These results provide additional evidence mapping the outward movement of the S4 segment through the gating pore in the voltage sensor during activation and further define the molecular basis for the voltage-dependent gating pore currents that cause hypokalemic and normokalemic periodic paralysis.

MATERIALS AND METHODS

Mutagenesis and expression in insect cells

NaChBac was originally cloned from *B. halodurans* (Ren et al., 2001). All clones in this study were made on the NaChBac WT channel in a p-thrombin expression vector, which is suitable for insect cells. Single-point mutations were done using PCR (QuikChange; Agilent Technologies). All mutants were verified by sequencing the mutated cDNA. NaChBac WT and mutant constructs were expressed in *Trichoplusia ni* insect cells using recombinant baculovirus generated using the Bac-to-Bac system (Life Technologies). Cells were infected and then incubated at 25–27°C for at least 24 h before measurement.

Electrophysiology

All constructs showed high expression, enabling us to measure gating current and gating pore currents 36–48 h after infection. Whole-cell sodium currents were recorded using an Axopatch 200 amplifier (Molecular Devices) with glass micropipettes (2–5 MΩ). Capacitance was subtracted and series resistance was compensated using internal amplifier circuitry; 80–85% of series resistance was compensated. For ionic current and some gating pore current measurements, intracellular pipette solution contained (mM) 35 NaCl, 105 CsF, 10 EGTA, and 10 HEPES, pH 7.4 (adjusted with CsOH). The extracellular solution contained (mM) 140 NaCl, 2 $CaCl_2$, 2 $MgCl_2$, and 10 HEPES, pH 7.4 (adjusted with NaOH). For R3C gating pore current measurements, the extracellular solution contained (mM) 70 NaCl, 70 guanidinium-sulfate, 2 $CaCl_2$, 2 $MgCl_2$, and 10 HEPES, pH 7.4 (adjusted with NaOH). For gating currents measurements, the intracellular pipette solution contained (mM) 140 NMDG-F, 5 choline-Cl, 10 NMDG-HEPES, and 10 NMDG-EGTA, pH 7.4 (adjusted with H_2SO_4). The extracellular solution contained (mM) 140 NMDG-$MeSO_3$ and 10 NMDG-HEPES, pH 7.4 (adjusted with H_2SO_4). Voltage clamp pulses were generated and currents were recorded using Pulse software controlling an Instrutech ITC18 interface (HEKA). Data were analyzed using Igor Pro 6.2 (WaveMetrics). When using a depolarized holding potential for gating charge or gating pore current measurements, the depolarized holding potential was maintained for 3–5 min before beginning measurements. All experiments were performed at room temperature (20–24°C).

Data analysis

Peak current versus voltage relationships were fit with $(V - V_{rev})/\{1 + \exp[(V - V_{1/2})/k]\}$, where V_{rev} is the apparent reversal potential, $V_{1/2}$ is the half-activation voltage, and k is a slope factor defined as RT/ZF, where R is the gas constant, T is absolute temperature, F is Faraday's number, and Z the apparent charge. Conductance-voltage relationships and charge-voltage relationships were fit with a Boltzmann function of the form $1/\{1 + \exp[(V - V_{1/2})/k]\}$. No leak subtraction protocols were applied during measurement of gating pore currents. For analysis of gating pore current, the current at the end of each pulse was measured. For R1C and R2C, the linear leak current at positive potentials where I_{gp} was minimal was fit with a line and subtracted from the total current. The remaining nonlinear component was taken as gating pore current. The current versus voltage relationship of the gating pore current was differentiated to yield G_{gp}-V relationships. For R3C, G_{gp} was generated as $I_{gp}/(V - V_{rev})$, where V is the step voltage and V_{rev} is the apparent reversal potential.

Gating currents were measured during 20-ms depolarizations from holding potentials of either 0 or −80 mV. This duration was adequate for NaChBac activation to reach steady-state with minimal inactivation (Fig. S1). For measurements from 0 mV, 20-ms-long hyperpolarizations to a series of potentials were applied. Leak subtraction pulses were applied from the 0-mV holding potential (P/10). For measurements from −80 mV, membrane potential was first stepped to −150 mV for 30 ms, and then steps to a series of test potentials were applied. Leak subtraction pulses were applied from a holding potential of 0 mV (P/4 or P/−4). For quantitative comparison, we always integrated the gating current in response to a depolarizing step. For depolarizations, the baseline at the end of the depolarization was subtracted from the trace and the gating current was integrated. For hyperpolarizations from 0 mV, the gating current transient upon returning to 0 mV after the pulse was integrated. Error bars in all figures represent SEM.

Online supplemental material

Fig. S1 presents the time course of NaChBac activation and inactivation when expressed in *T. ni* insect cells. Fig. S2 demonstrates equality of ON and OFF gating currents whether recorded using

a holding potential of −80 mV or a holding potential of 0 mV. Fig. S3 shows Rosetta models of three resting and three activated states of the voltage sensor. Online supplemental material is available at http://www.jgp.org/cgi/content/full/jgp.201411210/DC1.

RESULTS

Expression of NaChBac in insect cells

Insect cells from *T. ni* expressing WT NaChBac channels had large voltage-activated sodium currents (mean amplitude = 6 nA; Fig. 1, A and B) compared with those reported in mammalian cell expression systems (Ren et al., 2001). The activation curve measured from tail currents recorded upon repolarization to −150 mV ($n = 4$; Fig. 1 C) was fit by a Boltzmann equation with $V_{1/2}$ = −37 ± 0.7 mV and a slope factor k = 9.7 ± 0.4 mV. Activation curves fit using peak current-voltage relationships (Fig. 1 D) were comparable with those from recordings in mammalian cells in which solutions similar to ours were used (Chahine et al. [2004]: $V_{1/2}$ = −35.9 mV, k = 10.1 mV; DeCaen et al. [2008]: $V_{1/2}$ = −43 mV, k = 6.7 mV). Recovery from inactivation was best fit with a double exponential equation with τ_1 = 0.2 s (73% of current) and τ_2 = 1.34 s (27% of current; Fig. 1 E). The ability to obtain high expression levels of NaChBac in *T. ni* cells enabled us to measure gating charge movement accurately (Fig. 1 F). Gating charge movements were measured at two different holding potentials. We waited 3–5 min after the change in holding potential before making gating current measurements. From a holding potential of −80 mV, a short (30 ms) hyperpolarizing pulse to −150 mV was applied and the membrane potential was then depolarized in 10-mV steps. The gating charge movement measured from a holding potential of −80 mV was fit by a Boltzmann function with $V_{1/2}$ = −86.9 ± 1.7 mV, k = 15.8 ± 0.6 mV ($n = 5$; Fig. 1 F). In contrast, gating charge movement measured from a holding potential of 0 mV had a $V_{1/2}$ = −127.8 ± 5.6 mV, k = 14.4 ± 1.2 mV (Fig. 1 F). Whether measured from a holding potential of −80 mV or a holding potential of 0 mV, the charge that moved

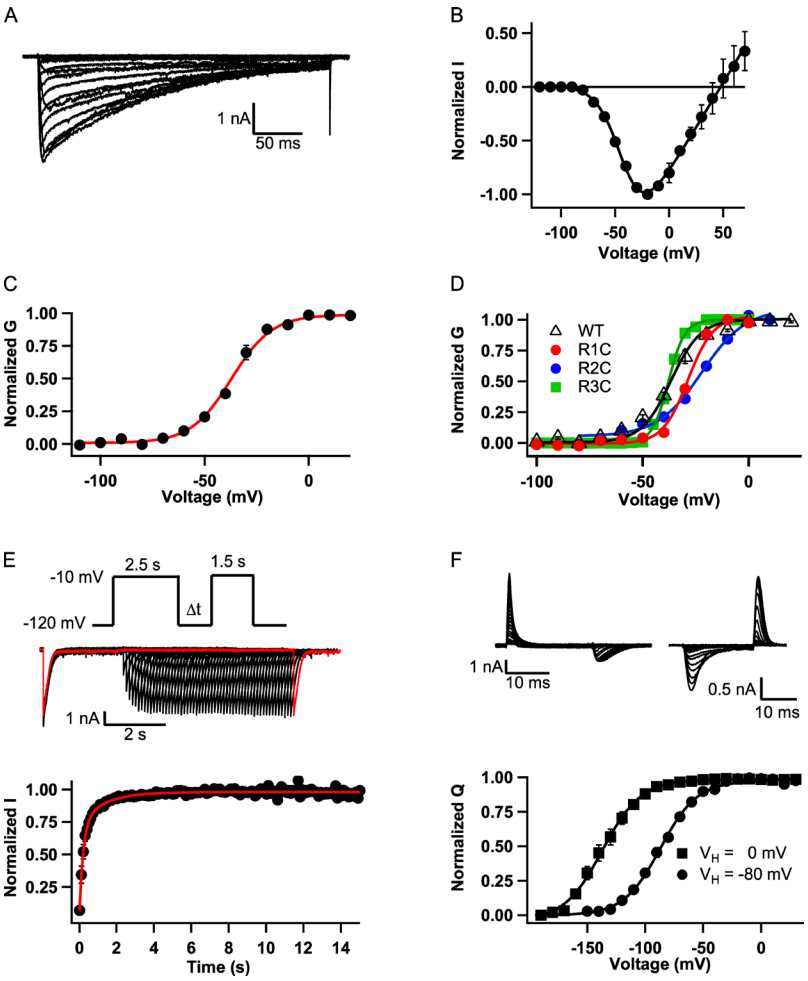

Figure 1. Biophysical properties of NaChBac WT expressed in *High 5* insect cells. (A) Representative ionic currents measured from NaChBac WT. The cell was held at −120 mV, and 300-ms depolarizations were applied to potentials from −120 to 50 mV in 10-mV increments. (B) I-V curve of NaChBac WT. (C) Voltage dependence of activation of NaChBac WT measured from peak tail currents with a $V_{1/2}$ = −36.6 ± 0.8 mV ($n = 4$). (D) G-V curves of WT, R1C, R2C, and R3C mutants derived from peak I-V relationships. The voltages for half-maximal channel activation and slope are WT: $V_{1/2}$ = −36.6 ± 0.8 mV, k = 7.00 ± 0.10 mV; R1C: $V_{1/2}$ = −22.2 ± 2.3 mV, k = 6.00 ± 0.62 mV; R2C: $V_{1/2}$ = −28.6 ± 0.7 mV, k = 10.39 ± 2.13 mV ($P < 0.05$ vs. WT); and R3C: $V_{1/2}$ = −37.8 ± 0.1 mV, k = 3.80 ± 0.12 mV ($P < 0.05$ vs. WT). (E) Recovery from inactivation of NaChBac WT. The cells were held at −120 mV, and a 2.5-s inactivation pulse to −10 mV was applied. A variable recovery interval was followed by a 1.5-s test pulse (protocol, top). (middle) Example superimposed current records are shown with the record from the trace with longest recovery interval shown in red. (bottom) Peak test pulse current was plotted versus recovery interval. Recovery from inactivation was best fit with a double exponential equation where τ_1 = 0.2 s, 73% of current and τ_2 = 1.34 s, 27% of current ($n = 7$). (F) Gating currents of NaChBac WT. Gating currents were measured using holding potentials of −80 or 0 mV. When the holding potential was −80 mV, a short (30 ms) prepulse to −150 mV was followed by 20-ms steps to more positive potentials in 10-mV increments before returning to −150 mV for 20 ms. When the holding potential was 0 mV, 20-ms pulses were applied to more hyperpolarized potentials. (top) Examples of gating current traces measured using the −80-mV holding potential (left) or the 0-mV holding potential (right). (bottom) Q-V relationships. The Q-V relationship measured from a holding potential of −80 mV has a $V_{1/2}$ = −86.9 ± 1.7 mV, k = 15.8 ± 0.6 mV ($n = 5$); that measured from a holding potential of 0 mV has a $V_{1/2}$ = −127.8 ± 5.6 mV, k = 14.4 ± 1.2 mV ($n = 5$). Error bars represent SEM.

in response to the pulse (ON gating current) and the charge that moved back at pulse termination (OFF gating current) were equal (Fig. S2). The large difference in the voltage dependence of gating charge movement when measured after a prolonged period at 0 mV, where all sodium channels are inactivated, versus −80 mV, where a large percentage of channels are in the resting state, illustrates a major hysteresis in voltage sensor function between the two holding potentials. Similar slow hysteresis of voltage sensor movement has been observed previously in studies of bacterial and eukaryotic sodium channels (Fernández et al., 1982; Kuzmenkin et al., 2004; Sokolov et al., 2008; Capes et al., 2012).

Gating pore currents of R1C and R2C

To induce gating pore current, the R1, R2, and R3 gating charges were mutated individually to Cys. Mutants R1C and R2C retained high-level expression and conductance activated with voltage dependence similar to WT (R1C: $V_{1/2} = -28.7 \pm 0.7$ mV; R2C: $V_{1/2} = -22.2 \pm 2.3$; Fig. 1 D). For R1C, measurement of gating charge movement using hyperpolarizing steps from a holding potential of 0 mV with NMDG-based solutions having minimal permeant ions yielded a Q-V curve with $V_{1/2} = -108 \pm 6.4$ mV, k = 23.8 ± 1.5 mV ($n = 6$), which approached saturation at −200 mV (Fig. 2, A and C [black]). From the same holding potential of 0 mV but using Na^+-containing solutions to measure ionic currents, application of hyperpolarizing voltage pulses in 10-mV increments induced steps in ionic current that became nonlinear and increasingly large negative to approximately −80 mV as the result of formation of an open gating pore through the voltage-sensing domain beyond this potential. The gating pore currents increased in amplitude with hyperpolarization until −200 mV (Fig. 2 B). The gating pore conductance was calculated by differentiating the gating pore current I-V curve to yield a G_{gp}-V curve (Fig. 2 C, red). The voltage dependences of inward movement of gating charge (Fig. 2 C, black) and activation of G_{gp} (Fig. 2 C, red) are closely correlated. These results indicate that the R1 gating charge is on the extracellular side of the gating pore when the voltage sensor is held at 0 mV and moves inward to take a position in or near the hydrophobic constriction site in the gating pore upon hyperpolarization (Fig. 2 D). In this position, the substituted Cys residue allows gating pore current conducted by cations moving inward through the gating pore. As the voltage sensor moves inward in response to hyperpolarizing potentials, gating pore current is first observed at approximately −90 mV, where ∼30% of the

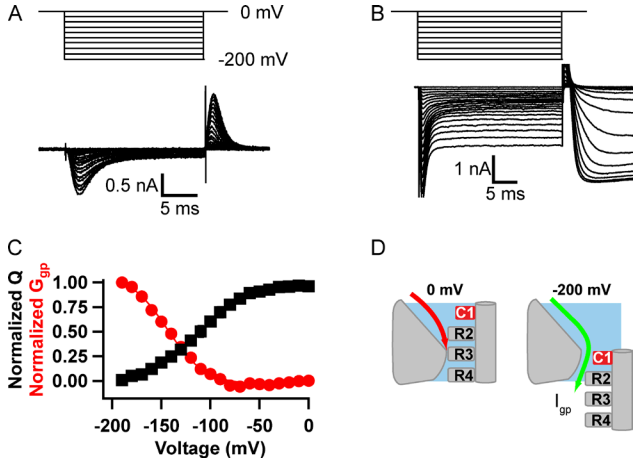

Figure 2. Voltage dependence of gating charge movement and gating pore opening of R1C measured from a holding potential of 0 mV. (A) Example of gating currents measured in a cell expressing R1C in response to hyperpolarizations from a holding potential of 0 mV. (B) Currents elicited in a cell expressing R1C by a series of hyperpolarizing pulses in 10-mV steps from a holding potential of 0 mV. No leak subtraction protocol was used. I_{gp} is the nonlinear current elicited by the hyperpolarizations and was measured at the end of the hyperpolarizing pulse. (C) The correlation of charge movement (Q-V: $V_{1/2} = -108 \pm 6.4$ mV, k = 23.84 ± 1.5 mV; $n = 6$) and gating pore conductance (G_{gp}: $V_{1/2} = -144.4 \pm 4.1$ mV, k = −21 ± 1.65 mV; $n = 8$) for NaChBac R1C. Gating pore conductance was determined by differentiating the I_{gp} versus voltage relationship (see Materials and methods). (D) A cartoon illustrating our interpretation of the results for R1C. R3 occupies and seals the gating pore at 0 mV. By hyperpolarizing to more negative potentials, S4 moves inward, bringing R1C into the critical position in the gating pore negative to approximately −80 mV.

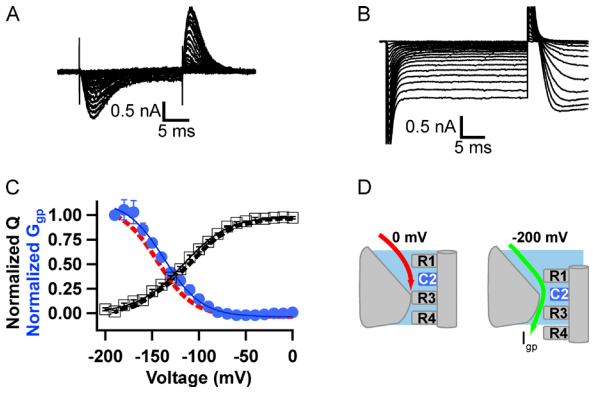

Figure 3. Voltage dependence of gating charge movement and gating pore opening of R2C measured from a holding potential of 0 mV. (A) Example of gating currents measured in a cell expressing R2C in response to hyperpolarizations from a holding potential of 0 mV. (B) R2C gating pore currents elicited by holding the cell at 0 mV and applying a series of hyperpolarizing pulses in 10-mV increments with no leak subtraction. I_{gp} was measured at the end of the pulse. (C) The correlation of charge movement (open squares; Q-V: $V_{1/2} = -115 \pm 3$ mV, k = 23.7 ± 0.6 mV; $n = 6$) and gating pore conductance (blue circles; G_{gp}: $V_{1/2} = -139.3 \pm 3.2$ mV, k = −21.6 ± 2.6 mV; $n = 5$) of NaChBac R2C mutant. The Q-V (black dashes) and G_{gp}-V (red dashes) relationships for R1C from Fig. 2 C are overlain for comparison. Error bars represent SEM. (D) A cartoon illustrating our interpretation of the results for R2C. R3 occupies and seals the gating pore at 0 mV. By hyperpolarizing to more negative potentials, S4 moves inward, bringing R2C into the critical position in the gating pore negative to approximately −90 mV.

remaining gating charge has been translocated through the hydrophobic constriction site. The presence of gating pore current indicates that the Cys substituted for R1 is in a position where R1 would normally be required to seal the gating pore (Fig. 2 D). The voltage dependence of G_{gp} shows that occupancy of the gating pore by R1C increases between −80 and −200 mV, with half-maximal activation ($V_{1/2}$) at −144 ± 4.1 mV, k = −21 ± 1.6 mV (n = 8), where ~80% of the gating charge of R2–R4 has moved inward. At −200 mV, the remaining gating charges have largely moved inward through the gating pore, and R1C is at or near the hydrophobic constriction site (Fig. 2 D). The G_{gp}-V relationship is expected to be negative with respect to the Q-V relationship because it reports only the last steps in inward S4 movement during deactivation, in which the gating pore is occupied by the Cys at the R1 position and the other gating charges have already passed through the gating pore.

From a holding potential of 0 mV, the return of the gating charge of the R2C mutant to its inward position followed a similar voltage dependence to that of R1C (Fig. 3, A and C [black]; $V_{1/2}$ = −115 ± 3 mV, k = 23.7 ± 0.6 mV; n = 6). Under these conditions, the inward gating pore current is first observed at approximately −90 mV (Fig. 3, B and C [blue]) and activates with a voltage dependence similar to the R1C mutant (Fig. 3 C, red). The voltage dependence of activation of G_{gp} for R2C ($V_{1/2}$ = −139.3 ± 3.2 mV, k= −21.6 ± 2.6 mV; n = 5) is similar to R1C ($V_{1/2}$ = −144.4 ± 4.1 mV; k = −21 ± 1.6 mV). These similar voltage dependences of G_{gp} for R1C and R2C indicate that the R1 and R2 gating charges share responsibility for sealing that gating pore over a broad range of voltages between −90 and −200 mV. Both gating charges may be needed in the hydrophobic constriction site to fully seal the gating pore at negative membrane potentials, or R1 and R2 may time-share occupancy of the gating pore in this voltage range. Our results indicate that, even though the R1 and R2 gating charges must pass through the gating pore sequentially as the S4 segment moves, the voltage dependence of their occupancy of the gating pore is quite similar.

Block of R1C and R2C gating pore current during activation

NaChBac channels are in the closed state at −80 mV (Fig. 1). To measure gating current from the closed state, cells were held at −80 mV and a short pulse (30 ms) to −150 mV was applied, followed by depolarizing pulses to a series of potentials in 10-mV intervals. The Q-V curves for both the R1C and R2C mutants show similar voltage dependence, with $V_{1/2}$ = −102.3 ± 6.9 mV, k = 28.6 ± 1.46 mV (n = 5) for R1C and $V_{1/2}$ = −95.2 ± 0.4 mV, k = 17 ± 0.8 mV (n = 4) for R2C (Fig. 4, A and B, black closed and open squares, respectively). Measurements of gating pore currents from a holding potential of −80 mV revealed that R1C has only a slight trend toward more negative voltage dependence of G_{gp} ($V_{1/2}$ = −160.3 ± 4.5 mV, k = −24.7 ± 3.7 mV for R1C [n = 10] vs. $V_{1/2}$ = −151.9 ± 3.9 mV, k = −24.5 ± 3.6 mV for R2C [n = 6]; $P < 0.2$). As with measurements from a 0-mV holding potential, gating pore current from a −80-mV holding potential is produced in either R1C or R2C mutant channels over a broad and overlapping voltage range and at potentials before substantial gating charge has transited the hydrophobic constriction site.

Gating pore currents of the R3C mutant

The voltage dependence of activation of the R3C mutant is similar to WT (Fig. 1 D). Gating charge movement was measured by holding the cell at 0 mV, where the voltage sensor is activated and the channel is in its slow-inactivated state. Hyperpolarizing voltage pulses cause deactivation and inward movement of the gating charge of the R3C mutant with slower kinetics than mutants

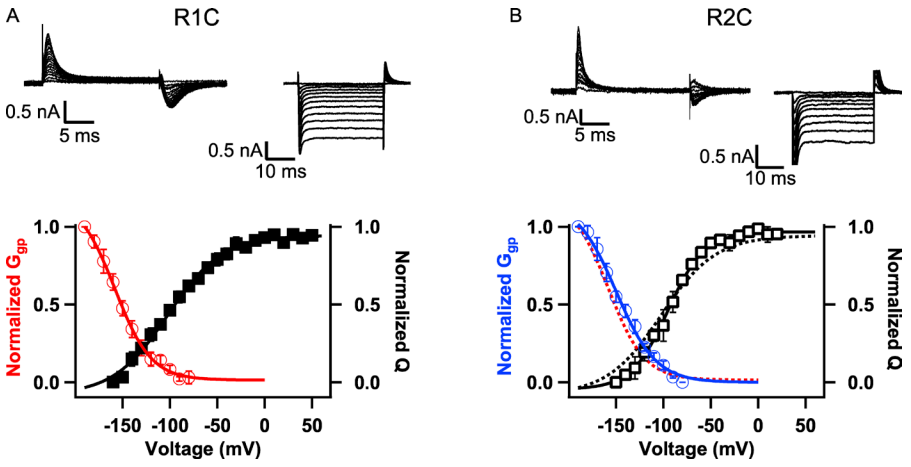

Figure 4. Voltage dependence of gating charge movement and gating pore opening of R1C and R2C measured from a holding potential of −80 mV. (A, top) Representative traces of gating currents (left) and gating pore currents (right) measured from a holding potential of −80 mV for R1C. Gating current traces were recorded after a 30-ms prepulse to −150 mV. (bottom) Correlation of charge movement (Q-V: $V_{1/2}$ = −102.3 ± 6.9 mV, k = 28.6 ± 1.46 mV; n = 5) and gating pore conductance (G_{gp}-V: $V_{1/2}$ = −160.3 ± 4.5 mV, k = −24.7 ± 3.7 mV; n = 10) of NaChBac R1C. (B, top) Representative traces of gating currents (left) and gating pore currents (right) measured from a holding potential of −80 mV for R2C. (bottom) Correlation of charge movement (Q-V: $V_{1/2}$ = −95.2 ± 0.4, k = 17 ± 0.8 mV; n = 4) and gating pore conductance (G_{gp}-V: $V_{1/2}$ = −151.9 ± 3.9 mV, k = −24.5 ± 3.6 mV; n = 6) of NaChBac R2C. R1C data from A are shown here as dashed lines for comparison. Error bars represent SEM.

R1C and R2C (Fig. 5 A). The following outward activation gating charge movement upon return to 0 mV was rapid, comparable with those observed with other mutants (Fig. 5 A). The voltage dependence of gating charge movement was similar to WT with $V_{1/2}$ = −130 ± 3.5 mV, k = 15.7 ± 0.6 mV (n = 5; Fig. 5, A and C [black]).

The R3C mutant showed only a small gating pore current with 140 mM NaCl as the major ionic species in the extracellular solution (not depicted). To measure larger gating pore currents, experiments with R3C were performed in extracellular solution containing 70 mM NaCl and 70 mM guanidinium sulfate because guanidinium has larger conductance through gating pores (Tombola et al., 2005; Sokolov et al., 2010). From a holding potential of 0 mV under these ionic conditions, I_{gp} of mutant R3C appears nearly instantaneously at all potentials (Fig. 5 B), reflecting gating pore current through the activated voltage sensor in the slow-inactivated state of the channel. However, at more negative membrane potentials (−130 to −200 mV), the gating pore current declines significantly during the hyperpolarizing pulse (Fig. 5 B). The voltage dependence of gating pore conductance recorded using a holding potential of 0 mV and measured at the end of the pulse is similar to that of gating charge movement (Fig. 5 C, green). Gating pore conductance is constant from 0 to approximately −110 mV and then declines at more negative potentials, with $V_{1/2}$ of G_{gp} = −140.9 ± 4.2 mV and k = 7.2 ± 0.28 mV (n = 6). These results for mutant R3C fit the model illustrated in Fig. 5 D. At 0 mV, R3C occupies the hydrophobic constriction site, and therefore it conducts gating pore current in this position. Hyperpolarization instantaneously increases gating pore current because the substituted Cys residue remains in the narrow part of the gating pore that is critical for conduction of inward gating pore current, and the current increases in response to the increase in driving force at more negative potentials. However, for strong hyperpolarizations, the S4 segment begins to move inward and reduces the amplitude of gating pore current by removing the substituted Cys residue from the hydrophobic constriction site. This inward movement of S4 is relatively slow, as reflected in the slow rate of decline of the gating pore current, perhaps because the neutral Cys residue occupies most of the region of the focused electrical field in the narrow part of the gating pore and thereby reduces the effect of voltage on S4 movement.

The components of the gating charge movement, ionic currents, and gating pore currents for mutant R3C are analyzed in more detail in Fig. 6. At the holding potential of 0 mV, the voltage sensors are in an activated conformation, and the channels have entered the slow-inactivated state. Upon hyperpolarization from 0 mV (Fig. 6 A, (1)), inward gating pore current increases instantaneously as the result of the increase in driving force. Decay is more rapid and complete at more hyperpolarized voltages, as illustrated for steps to −110 (red), −150 (blue), and −170 mV (green). The channels also recover from slow inactivation at these hyperpolarized potentials. Return to the holding potential of 0 mV causes outward movement of the S4 gating charges, which is accompanied by a transient outward current that activates and decays in a few milliseconds upon depolarization from all hyperpolarized voltages (Fig. 6 A, (2)). As subtraction of capacity transients cannot be used in gating pore current experiments, this second current transient reflects outward gating charge movement contaminated by some uncompensated capacity

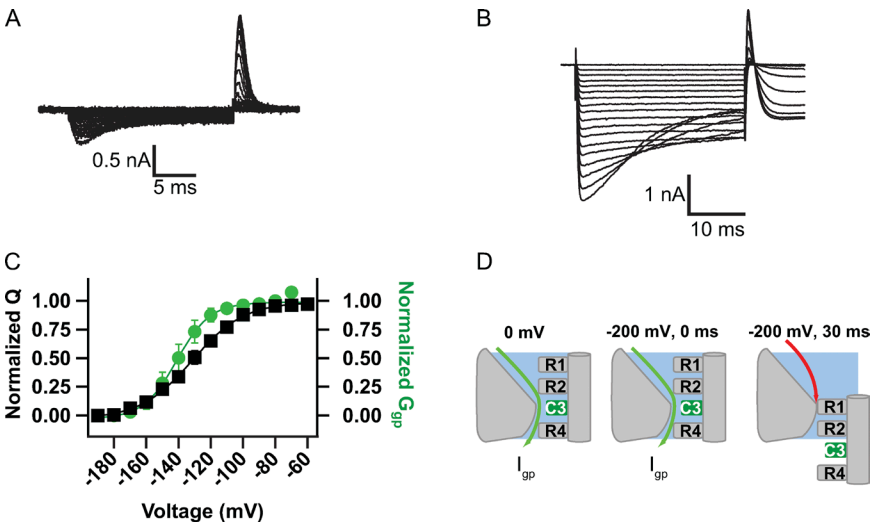

Figure 5. Gating current and gating pore measurements for R3C from a holding potential of 0 mV. (A) Gating currents induced by hyperpolarizations from a holding potential of 0 mV. Steps were increased in 10-mV increments. (B) Gating pore currents elicited by holding the cell at 0 mV and applying hyperpolarizing pulses in 10-mV increments with no leak subtraction. I_{gp} was measured at the end of the pulse. (C) The correlation of charge movement (Q-V: $V_{1/2}$ = −129.6 ± 3.47 mV, k = 15.7 ± 0.6 mV; n = 5) and gating pore conductance (G_{gp}-V: $V_{1/2}$ = −140.9 ± 4.2 mV, k = 7.2 ± 0.28 mV; n = 6) of NaChBac-R3C. Gating pore voltage dependence and gating charge voltage dependence track each other. Error bars represent SEM. (D) Cartoon illustrating our interpretation of the results. At 0 mV, R3C is located in the gating pore (left). Immediately upon hyperpolarization to −180 mV, inward gating pore current is increased by the increase in driving force for inward ion movement (middle). During the hyperpolarization to −180 mV, the S4 segment slowly translates inward, moving R2 into the critical point of the gating pore and terminating gating pore current (right).

transient. Nevertheless, as expected from the voltage dependence of gating charge movement (Fig. 5 C), this outward transient is first observed at −110 mV (Fig. 6 A, (2), red trace) and becomes progressively larger with more negative holding potentials up to −170 mV (Fig. 6 A, (2), green trace) as the fraction of voltage sensors that were driven into the resting state during hyperpolarization increases. The outward transients caused by reactivation of the voltage sensors are followed by activation of the inward central pore current (Fig. 6 A, (3)), which is observed as a sustained inward current after the transient outward gating/linear capacity current. This central pore current also is first observed after hyperpolarization to −110 mV (Fig. 6 A, (3), red trace) and reaches maximum after hyperpolarization to −170 mV (Fig. 6 A, (3), green trace) because a greater fraction of the voltage sensors return to their resting state and recover from inactivation with increasing hyperpolarization. Thus, the voltage sensors that have recovered from inactivation upon repolarization can be activated again and generate central pore current.

To be certain that the inward gating pore current is not contaminated by central pore current, we blocked the central pore with nifedipine, which is a known blocker of NaChBac channels (Ren et al., 2001). Nifedipine did not change the amplitude, voltage dependence, or kinetics of the gating pore current (Fig. 6 B). In contrast, it completely blocked the inward central pore current that appears after return to 0 mV (Fig. 6 B, arrows). The gating pore currents are similar in magnitude whether or not nifedipine is present (Fig. 6 C). These results confirm our identification of gating pore current and central pore current as the first and third current components in these experiments. Altogether, this analysis supports the conclusion that the R3 gating charge is located in the narrow focused field in the hydrophobic constriction site in the gating pore at 0 mV, such that the R3C mutant conducts gating pore current in the activated state of the voltage sensor in the open and slow-inactivated states of the channel. R3 moves inward upon hyperpolarization to return the voltage sensor to its resting state and terminate gating pore current.

DISCUSSION

Gating pore currents in somatic cells

Previous studies of gating pore currents have used the *Xenopus laevis* oocyte expression system and the cut-open oocyte preparation for voltage clamp because of the large number of sodium channels required to observe small gating pore currents (e.g., Sokolov et al., 2005, 2007; Struyk and Cannon, 2007; Gamal El-Din et al., 2008). Our results show that expression of bacterial sodium channels in insect cells, using methods developed for structural biology, allows high-fidelity recording of gating pore currents in parallel with gating charge movement and ionic currents through the central pore. Moreover, because mutations are represented in all four identical subunits of NaChBac and other bacterial sodium channels, quantitative comparison of gating charge movement and gating pore current can be readily made. In contrast, in previous studies of mammalian sodium channels by us and others, the gating pore currents generated by mutations made in one of the four voltage sensors cannot easily be correlated with gating charge movements that are occurring in the voltage sensors in all four domains during the activation process. Thus, this new expression system has important technical advantages and is ideal for correlation of measurements

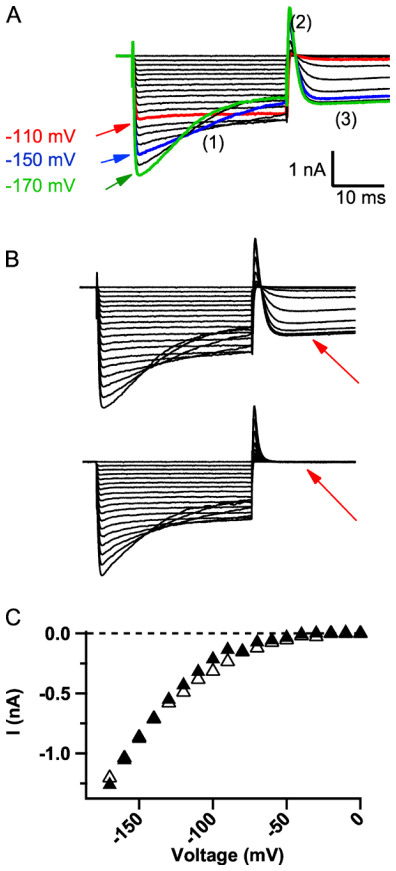

Figure 6. Separation of gating pore current and central pore current for NaChBac R3C using blockers and inactivation. (A) Current traces like those in Fig. 4 B showing the decline in I_{gp} during steps to strongly hyperpolarized potentials. Colors and associated arrows indicate currents recorded at the indicated potentials, and numbers in parentheses highlight particular phases of each trace. Phase 1, inward gating pore current; phase 2, outward gating charge movement plus residual capacity transient; phase 3, inward central pore current. (B) Nifedipine block. An experiment like the one in A was performed in the absence (top) and presence (bottom) of 100 µM nifedipine. Arrows denote the central pore current. (C) Gating pore current at the beginning of the pulse is plotted in the absence (open triangles) and presence (closed triangles) of nifedipine.

of gating pore currents, gating charge movement, and ionic currents with structural studies.

Structural transitions in the NaChBac voltage sensor

We have previously probed the positions of the gating charges of NaChBac using the disulfide locking method and shown that they move outward and exchange ion pair partners upon depolarization (DeCaen et al., 2008, 2009, 2011). High-resolution models of three resting states and three activated states of the voltage sensor were developed using the Rosetta ab initio modeling algorithm to fit these experimental results (Yarov-Yarovoy et al., 2012). In these models, progressive depolarization forces the S4 segment to move outward through the hydrophobic constriction site at the center of the voltage sensor, exchanging ionic and hydrogen-bonding interactions with the intracellular negative cluster for energetically similar interactions with the extracellular negative charge cluster (Fig. S3). Activated state 2 of NaChBac is very similar in conformation to the activated state of the voltage sensor observed in the crystal structure of Na_VAb (Payandeh et al., 2011, 2012). Below we consider our results presented in this study in terms of these six functional states of the voltage sensor in NaChBac.

R1 and R2 occupy and seal the gating pore in resting states

The R1C and R2C mutants have similar voltage dependence of charge movement and gating pore conductance (Figs. 2 and 3). These results indicate that either the side chain of the amino acid at the position of R1 or that at position R2 can occupy the hydrophobic constriction site in the gating pore in one or more resting states of the voltage sensor. Comparison with the structural models of three resting states of the voltage sensor (Fig. S3) reveals that the R1 and R2 gating charges reside in or near the hydrophobic constriction site in resting states 1 and 2. Movement of the voltage sensor between these two resting states may underlie the requirement for both R1 and R2 to effectively prevent gating pore current in the resting state of the channel.

Chemical modification experiments have shown that R1C and R2C in NaChBac mutants are both accessible for reaction with MTSES from extracellular solution in the closed state of the channel (Blanchet and Chahine, 2007). Moreover, R2C could also be modified from the intracellular solution when the channel was closed. This suggests that R2C can visit positions both extracellular and intracellular to the hydrophobic constriction site, even when the membrane potential is strongly negative (Blanchet and Chahine, 2007). These results indicate that R1C precedes R2C as the side chains of the S4 segment transit the gating pore, but both residues can occupy the gating pore in resting states. These results are also consistent with the idea that the voltage sensor can move between resting states 1 and 2 at negative membrane potentials, which would allow labeling of R1C from the extracellular milieu and R2C from both intracellular and extracellular solutions (Fig. S3).

Our Rosetta models of NaChBac show the gating charge residues in the hydrophobic constriction site in a 3_{10}-helix conformation in all six states, as if the 3_{10}-helix conformation is formed as the S4 segment moves outward through the hydrophobic constriction site and relaxes later as the pore opens (Fig. S3; Yarov-Yarovoy et al., 2012). The crystal structure of Na_VAb (Payandeh et al., 2011, 2012) shows that the entire S4 segment can adopt a 3_{10}-helix conformation. However, the 3_{10}-helix is partially relaxed to an α helix in the more outward conformation of the S4 segment of the voltage sensor of the Na_VRh structure (Zhang et al., 2012), as predicted by the Rosetta models (Fig. S3; Yarov-Yarovoy et al., 2012). The 3_{10}-helix conformation of the S4 segment places the arginine gating charges in a linear array in the hydrophobic constriction site and thus would reduce energy barriers for exchange of R1 and R2 across the hydrophobic constriction site of the gating pore during transitions between energetically similar resting states and place the substituted Cys residues in an optimum position for conductance of gating pore current.

R3 seals the gating pore in an activated state

The Na_VAb crystal structure (Payandeh et al., 2011) shows that Cα of R3 occupies the hydrophobic constriction site and its positively charged side chain fills the innermost tip of the aqueous cleft on the extracellular side of the hydrophobic constriction site in an activated state, similar to activated state 2 of NaChBac (Fig. S3). The side chain of R3 is pointing toward the extracellular surface, whereas the side chain of R4 is angled intracellularly. Our results indicate that R3 moves inward, out of the hydrophobic constriction site, at hyperpolarized membrane potentials, leading to loss of gating pore current for R3C. At the same time, R1 and R2 move inward and occlude the hydrophobic constriction site in the gating pore at more hyperpolarized potentials. The time constant of deactivation of I_{gp} in the R3C mutant (∼12 ± 0.9 ms; $n = 7$) is similar to the time constant of the decay of the deactivation component of gating charge movement measured at the same potential (∼7.23 ± 0.23 ms; $n = 6$). This movement is likely to resemble the conformational changes that occur during transition from activated state 2 to resting state 2 in our Rosetta model (Fig. S3). A study using site-directed spin labeling and electron paramagnetic resonance spectroscopy on the isolated VSD of NaChBac has shown that R3 is located in the narrowest region between the inward and outward vestibules in the activated state (Chakrapani et al., 2010), which fits well with our gating pore current results.

R3C continues to conduct gating pore current at the most positive potentials, much as R1C and R2C conduct gating pore current even at the most negative potentials. These results show that WT R3 occupies the gating pore

and seals it even at the most positive potentials sampled. Thus, the R3 side chain appears to be necessary to seal the gating pore over a broad range of depolarized voltages.

Sequential movement of gating charges through the gating pore during activation

Our experiments provide the first view of single gating charges moving through the gating pore in a voltage sensor based on measurements of gating pore current, because previous work on gating pore currents in potassium channels focused on mutations of only the R1 gating charge or on mutations of pairs of gating charges (Tombola et al., 2005; Gamal El-Din et al., 2010). We find that the R1 and R2 gating charges share interactions in or near the hydrophobic constriction site in resting states, but they move outward and allow entry of the R3 gating charge into the hydrophobic constriction site in the activated state. These results provide direct support for a sliding-helix mechanism of movement of the S4 segment and the gating charges during activation (Catterall, 2000, 2010).

Role of gating charges in the voltage dependence of charge movement

The mutation R1C virtually abolished the slow, holding potential–dependent hysteresis in the voltage dependence of charge movement that is observed for NaChBac (Fig. 1 and Table 1) and for all voltage sensors (Fernández et al., 1982; Kuzmenkin et al., 2004; Sokolov et al., 2008; Capes et al., 2012; Lacroix et al., 2012) because the voltage dependence of gating charge movement was similar when tested from holding potentials of 0 and −80 mV (quantified as ΔΔG in Table 1). R2C also reduced this hysteresis of gating charge movement (Table 1). These results suggest that when the voltage sensor is depolarized for a prolonged period of time, the native arginine side chains of the R1 and R2 residues make new interactions that stabilize the activated state of the voltage sensor, and these new interactions are required to produce the observed voltage shift.

Three structures of activated voltage sensors have been reported for bacterial sodium channels. In two of them (Payandeh et al., 2011, 2012), R1 interacts with residues in the S3 segment (Na_VAb Glu96 and Thr91) of the voltage sensor of the same subunit. In the third structure, Na_VRh (Zhang et al., 2012), R1 has a different disposition, interacting with Thr149 and Ile153 of S5 of the adjacent subunit (Zhang et al., 2012). R1 can make this interaction because the overall conformation of the voltage sensor is different in Na_VRh than in the two Na_VAb structures (Payandeh et al., 2011, 2012; Zhang et al., 2012). In Na_VAb, the entire length of the S4 is found in a 3_{10}-helical structure with the Arg side chains arranged on one face of the helix pointing toward the core of the voltage-sensing domain. In the Na_VRh structure, S4 is approximately one helical turn further outward relative to the rest of the voltage sensor than in the Na_VAb structures, and the outer segment of S4 has adopted an α-helical conformation, placing R1 in S4 near the external surface of the voltage sensor facing the pore domain, where it can interact with I153 and T149 of S5 (Zhang et al., 2012). Na_VRh has been proposed to be an NaChBac-like channel in an inactivated conformation (Zhang et al., 2012). Perhaps this conformation is stabilized in the slow-inactivated state of NaChBac; mutating R1 to Cys in R1C would prevent this interaction and abolish the stabilization of the voltage sensor in an activated state.

Voltage-dependent opening and closing of mutant gating pores in periodic paralysis

The pathophysiology of hypokalemic and normokalemic periodic paralysis is affected in an important way by the voltage dependence of gating pore opening and closing. Mutations at the R1 and R2 gating charges cause hypokalemic periodic paralysis by generating a leak pathway for Na^+ through the mutant voltage sensor in the resting state. Our structural models of resting states 1 and 2 illustrate how these gating charges block the gating pore in the resting state (Fig. S3). Mutation of those gating charges to smaller hydrophilic residues like cysteine would create a leak in the resting state, which would be closed by outward movement of the voltage sensor and occupancy of the hydrophobic constriction

TABLE 1

Relative apparent free energies of channel activation at hyperpolarized and depolarized holding potentials

Channel	$V_{1/2}$ (0 mV)	Z (0 mV)	ΔG (0 mV)	$V_{1/2}$ (−80 mV)	Z (−80 mV)	ΔG (−80 mV)	ΔΔG
	mV		*kcal/mol*	*mV*		*kcal/mol*	*kcal/mol*
WT	−127.8 ± 5.6	−1.9 ± 0.1	−5.4 ± 0.2	−86.9 ± 1.7	−1.6 ± 0.0	−3.3 ± 0.1	2.10
R1C	−108.8 ± 6.5	−1.1 ± 0.1	−2.7 ± 0.1	−102.3 ± 6.9	−0.9 ± 0.0	−2.4 ± 0.1	0.38
R2C	−115.7 ± 3.0	−1.0 ± 0.0	−2.9 ± 0.1	−95.2 ± 0.4	−1.3 ± 0.2	−3.0 ± 0.2	0.02
R3C	−129.6 ± 3.0	−1.6 ± 0.0	−4.9 ± 0.2	−105.3 ± 0.2	−1.4 ± 0.2	−3.3 ± 0.4	1.62

Apparent free energy for a two-state model, ΔG, was calculated as a measure for comparing the relative energies of opening WT and mutant channels at holding potentials of 0 or −80 mV as $\Delta G = -ZFV_{1/2}$. Z was the apparent charge, $V_{1/2}$ the half-activation voltage of charge movement, and F, Faraday's number (23.061 kcal per volt gram equivalent). The parameters $V_{1/2}$ and Z were calculated by using the slopes of fits of $1/(1 + \exp[RT(V - V_{1/2})/ZF]$ to Q-V curves, where R is the universal gas constant, T is temperature in °K, F is the Faraday constant, and Z is the valence. ΔΔG was calculated as ΔΔG = ΔG (−80 mV) − ΔG (0 mV).

site by R3 (Fig. S3). Similarly, our model of activated state 3 illustrates how the R3 gating charge that is mutated in normokalemic periodic paralysis blocks the gating pore in an activated state (Fig. S3). Mutation of this gating charge creates a leak in the activated state of the voltage sensor, which is present in both activated and slow-inactivated states of the channel (Sokolov et al., 2008). These results give a clear structural picture of the mechanism through which mutations of the R1–R3 gating charges to small hydrophilic residues can cause pathogenic gating pore current. Further elucidation of the structures of these mutant gating pores may come from crystal structures of the mutant $Na_V1.4$ channel in the future.

This research was supported by research grants R01 NS015751 and R01 HL112808 from the National Institutes of Health to W.A. Catterall.

The authors declare no competing financial interests.

Kenton J. Swartz served as editor.

Submitted: 11 April 2014
Accepted: 7 July 2014

REFERENCES

Bezanilla, F. 2000. The voltage sensor in voltage-dependent ion channels. *Physiol. Rev.* 80:555–592.

Blanchet, J., and M. Chahine. 2007. Accessibility of four arginine residues on the S4 segment of the *Bacillus halodurans* sodium channel. *J. Membr. Biol.* 215:169–180. http://dx.doi.org/10.1007/s00232-007-9016-1

Capes, D.L., M. Arcisio-Miranda, B.W. Jarecki, R.J. French, and B. Chanda. 2012. Gating transitions in the selectivity filter region of a sodium channel are coupled to the domain IV voltage sensor. *Proc. Natl. Acad. Sci. USA.* 109:2648–2653. http://dx.doi.org/10.1073/pnas.1115575109

Catterall, W.A. 2000. From ionic currents to molecular mechanisms: the structure and function of voltage-gated sodium channels. *Neuron.* 26:13–25. http://dx.doi.org/10.1016/S0896-6273(00)81133-2

Catterall, W.A. 2010. Ion channel voltage sensors: structure, function, and pathophysiology. *Neuron.* 67:915–928. http://dx.doi.org/10.1016/j.neuron.2010.08.021

Chahine, M., S. Pilote, V. Pouliot, H. Takami, and C. Sato. 2004. Role of arginine residues on the S4 segment of the *Bacillus halodurans* Na^+ channel in voltage-sensing. *J. Membr. Biol.* 201:9–24. http://dx.doi.org/10.1007/s00232-004-0701-z

Chakrapani, S., P. Sompornpisut, P. Intharathep, B. Roux, and E. Perozo. 2010. The activated state of a sodium channel voltage sensor in a membrane environment. *Proc. Natl. Acad. Sci. USA.* 107:5435–5440. http://dx.doi.org/10.1073/pnas.0914109107

Conti, F., and W. Stühmer. 1989. Quantal charge redistributions accompanying the structural transitions of sodium channels. *Eur. Biophys. J.* 17:53–59.

DeCaen, P.G., V. Yarov-Yarovoy, Y. Zhao, T. Scheuer, and W.A. Catterall. 2008. Disulfide locking a sodium channel voltage sensor reveals ion pair formation during activation. *Proc. Natl. Acad. Sci. USA.* 105:15142–15147. http://dx.doi.org/10.1073/pnas.0806486105

DeCaen, P.G., V. Yarov-Yarovoy, E.M. Sharp, T. Scheuer, and W.A. Catterall. 2009. Sequential formation of ion pairs during activation of a sodium channel voltage sensor. *Proc. Natl. Acad. Sci. USA.* 106:22498–22503. http://dx.doi.org/10.1073/pnas.0912307106

DeCaen, P.G., V. Yarov-Yarovoy, T. Scheuer, and W.A. Catterall. 2011. Gating charge interactions with the S1 segment during activation of a Na^+ channel voltage sensor. *Proc. Natl. Acad. Sci. USA.* 108:18825–18830. http://dx.doi.org/10.1073/pnas.1116449108

Fernández, J.M., F. Bezanilla, and R.E. Taylor. 1982. Distribution and kinetics of membrane dielectric polarization. II. Frequency domain studies of gating currents. *J. Gen. Physiol.* 79:41–67. http://dx.doi.org/10.1085/jgp.79.1.41

Gamal El-Din, T.M., D. Grögler, C. Lehmann, H. Heldstab, and N.G. Greeff. 2008. More gating charges are needed to open a Shaker K^+ channel than are needed to open an rBIIA Na^+ channel. *Biophys. J.* 95:1165–1175. http://dx.doi.org/10.1529/biophysj.108.130765

Gamal El-Din, T.M., H. Heldstab, C. Lehmann, and N.G. Greeff. 2010. Double gaps along Shaker S4 demonstrate omega currents at three different closed states. *Channels (Austin).* 4:93–100. http://dx.doi.org/10.4161/chan.4.2.10672

Hille, B. 2001. Ionic channels of excitable membranes. Third edition. Sinauer Associates, Sunderland, MA. 814 pp.

Hirschberg, B., A. Rovner, M. Lieberman, and J. Patlak. 1995. Transfer of twelve charges is needed to open skeletal muscle Na^+ channels. *J. Gen. Physiol.* 106:1053–1068. http://dx.doi.org/10.1085/jgp.106.6.1053

Kuzmenkin, A., F. Bezanilla, and A.M. Correa. 2004. Gating of the bacterial sodium channel, NaChBac: Voltage-dependent charge movement and gating currents. *J. Gen. Physiol.* 124:349–356. http://dx.doi.org/10.1085/jgp.200409139

Lacroix, J.J., S.A. Pless, L. Maragliano, F.V. Campos, J.D. Galpin, C.A. Ahern, B. Roux, and F. Bezanilla. 2012. Intermediate state trapping of a voltage sensor. *J. Gen. Physiol.* 140:635–652. http://dx.doi.org/10.1085/jgp.201210827

Long, S.B., E.B. Campbell, and R. MacKinnon. 2005. Crystal structure of a mammalian voltage-dependent Shaker family K^+ channel. *Science.* 309:897–903. http://dx.doi.org/10.1126/science.1116269

Long, S.B., X. Tao, E.B. Campbell, and R. MacKinnon. 2007. Atomic structure of a voltage-dependent K^+ channel in a lipid membrane-like environment. *Nature.* 450:376–382. http://dx.doi.org/10.1038/nature06265

Payandeh, J., T. Scheuer, N. Zheng, and W.A. Catterall. 2011. The crystal structure of a voltage-gated sodium channel. *Nature.* 475:353–358. http://dx.doi.org/10.1038/nature10238

Payandeh, J., T.M. Gamal El-Din, T. Scheuer, N. Zheng, and W.A. Catterall. 2012. Crystal structure of a voltage-gated sodium channel in two potentially inactivated states. *Nature.* 486:135–139.

Ren, D., B. Navarro, H. Xu, L. Yue, Q. Shi, and D.E. Clapham. 2001. A prokaryotic voltage-gated sodium channel. *Science.* 294:2372–2375. http://dx.doi.org/10.1126/science.1065635

Sokolov, S., T. Scheuer, and W.A. Catterall. 2005. Ion permeation through a voltage-sensitive gating pore in brain sodium channels having voltage sensor mutations. *Neuron.* 47:183–189. http://dx.doi.org/10.1016/j.neuron.2005.06.012

Sokolov, S., T. Scheuer, and W.A. Catterall. 2007. Gating pore current in an inherited ion channelopathy. *Nature.* 446:76–78. http://dx.doi.org/10.1038/nature05598

Sokolov, S., T. Scheuer, and W.A. Catterall. 2008. Depolarization-activated gating pore current conducted by mutant sodium channels in potassium-sensitive normokalemic periodic paralysis. *Proc. Natl. Acad. Sci. USA.* 105:19980–19985. http://dx.doi.org/10.1073/pnas.0810562105

Sokolov, S., T. Scheuer, and W.A. Catterall. 2010. Ion permeation and block of the gating pore in the voltage sensor of $Na_V1.4$ channels with hypokalemic periodic paralysis mutations. *J. Gen. Physiol.* 136:225–236. http://dx.doi.org/10.1085/jgp.201010414

Starace, D.M., and F. Bezanilla. 2004. A proton pore in a potassium channel voltage sensor reveals a focused electric field. *Nature.* 427:548–553. http://dx.doi.org/10.1038/nature02270

Struyk, A.F., and S.C. Cannon. 2007. A Na^+ channel mutation linked to hypokalemic periodic paralysis exposes a proton-selective gating

pore. *J. Gen. Physiol.* 130:11–20. http://dx.doi.org/10.1085/jgp.200709755

Stühmer, W., F. Conti, H. Suzuki, X.D. Wang, M. Noda, N. Yahagi, H. Kubo, and S. Numa. 1989. Structural parts involved in activation and inactivation of the sodium channel. *Nature.* 339:597–603. http://dx.doi.org/10.1038/339597a0

Tombola, F., M.M. Pathak, and E.Y. Isacoff. 2005. Voltage-sensing arginines in a potassium channel permeate and occlude cation-selective pores. *Neuron.* 45:379–388. http://dx.doi.org/10.1016/j.neuron.2004.12.047

Yang, N., and R. Horn. 1995. Evidence for voltage-dependent S4 movement in sodium channels. *Neuron.* 15:213–218. http://dx.doi.org/10.1016/0896-6273(95)90078-0

Yang, N., A.L. George Jr., and R. Horn. 1996. Molecular basis of charge movement in voltage-gated sodium channels. *Neuron.* 16:113–122. http://dx.doi.org/10.1016/S0896-6273(00)80028-8

Yarov-Yarovoy, V., P.G. DeCaen, R.E. Westenbroek, C.Y. Pan, T. Scheuer, D. Baker, and W.A. Catterall. 2012. Structural basis for gating charge movement in the voltage sensor of a sodium channel. *Proc. Natl. Acad. Sci. USA.* 109:E93–E102. http://dx.doi.org/10.1073/pnas.1118434109

Zhang, X., W. Ren, P. DeCaen, C. Yan, X. Tao, L. Tang, J. Wang, K. Hasegawa, T. Kumasaka, J. He, et al. 2012. Crystal structure of an orthologue of the NaChBac voltage-gated sodium channel. *Nature.* 486:130–134.